Toward a quantum-mechanical description of metal-assisted phosphoryl transfer in pyrophosphatase

P. Heikinheimo*†, V. Tuominen*‡, A.-K. Ahonen*§, A. Teplyakov¶, B. S. Cooperman‖, A. A. Baykov**, R. Lahti‡, and A. Goldman*‡§††

*Center for Biotechnology, PL 123, FIN-20521 Turku, Finland; ‡Department of Biochemistry, University of Turku, FIN-20014 Turku, Finland; §Institute of Biotechnology, University of Helsinki, PL 56, FIN-00014 Helsinki, Finland; ¶European Molecular Biology Laboratory, Deutsches Elektronen Synchrotron, D-22603 Hamburg, Germany; ‖Department of Chemistry, University of Pennsylvania, Philadelphia, PA 19104; and **AN Belozersky Institute of Physico-Chemical Biology, Moscow State University, Moscow 119899, Russia

Communicated by Thomas A. Steitz, Yale University, New Haven, CT, December 22, 2000 (received for review August 31, 2000)

The wealth of kinetic and structural information makes inorganic pyrophosphatases (PPases) a good model system to study the details of enzymatic phosphoryl transfer. The enzyme accelerates metal-complexed phosphoryl transfer 10^{10}-fold: but how? Our structures of the yeast PPase product complex at 1.15 Å and fluoride-inhibited complex at 1.9 Å visualize the active site in three different states: substrate-bound, immediate product bound, and relaxed product bound. These span the steps around chemical catalysis and provide strong evidence that a water molecule (O_{nu}) directly attacks PPi with a pK_a vastly lowered by coordination to two metal ions and D117. They also suggest that a low-barrier hydrogen bond (LBHB) forms between D117 and O_{nu}, in part because of steric crowding by W100 and N116. Direct visualization of the double bonds on the phosphates appears possible. The flexible side chains at the top of the active site absorb the motion involved in the reaction, which may help accelerate catalysis. Relaxation of the product allows a new nucleophile to be generated and creates symmetry in the elementary catalytic steps on the enzyme. We are thus moving closer to understanding phosphoryl transfer in PPases at the quantum mechanical level. Ultra-high resolution structures can thus tease out overlapping complexes and so are as relevant to discussion of enzyme mechanism as structures produced by time-resolved crystallography.

Inorganic pyrophosphatases (PPases) catalyze one of the oldest and most common reactions in cells and provide a good system for detailed analysis of enzymatic phosphoryl transfer from polyphosphate to water. The kinetics are well characterized (1, 2) and high-resolution structures are available along the reaction pathway (3). The enzyme accelerates hydrolysis of metal complexed inorganic pyrophosphate by 10^{10} compared with the uncatalyzed reaction (1)—but for PPases, as for enzymes in general, the exact source of rate enhancement remains unclear.

The original model of catalysis suggested that the mechanism proceeded in four steps with all steps after substrate binding partially rate-determining (1). The nucleophile, which is generated by coordinating a water molecule (O_{nu}) to two metal ions and which is further strengthened by donating a hydrogen bond to D117, is one key to pyrophosphate hydrolysis in PPases. In addition, the substrate pK_a is adjusted by extensive coordination to charged atoms (positively charged side chains and M^{2+}; ref. 3).

Our most recent solution studies (P. Halonen, unpublished data; refs. 2 and 4) indicate that the enzyme-substrate complex (EM_2:MPPi or EM_2:M_2PPi) undergoes isomerization during the catalytic cycle (Scheme 1; ref. 4). In addition, fluoride inhibition studies (4) are consistent with structural studies (3, 5) suggesting that the nucleophile is coordinated to D117.

We earlier determined the structure of complexes **A** and **E** (Scheme 1), but now have direct structural information on the mechanistically key intermediates **C** and **D**, as well as much higher resolution information on **E**. PPase is specifically inhibited by fluoride ion, which blocks the **C** to **D** conversion (4). We report the 1.9-Å crystal structure of the fluoride-inhibited substrate complex and the 1.15-Å structure of the product complex of yeast PPase. Based on these structures we suggest that low barrier hydrogen bonds (LBHBs), proton tunneling, and active site preorganization are important in rate enhancement in at least this class of metal-dependent phosphoryl transferases.

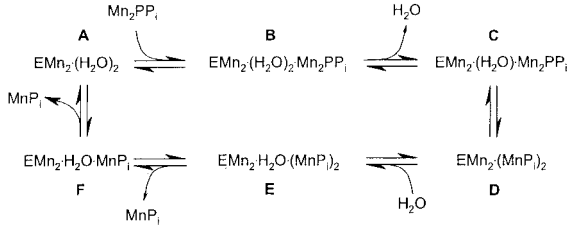

Scheme 1.

Materials and Methods

Crystallization and Data Collection. Protein purification and crystallization (3) and flash-freezing (5) for PPase:Pi_2 were as described. The 20–1.5-Å data were collected at $\lambda = 0.891$ Å and data from 2.5–1.15 Å from a second crystal at $\lambda = 0.901$ Å at Deutsches Elektronen Synchrotron (DESY). Frames were integrated and scaled in HKL (6). PPase:FPPi crystals were grown in 19 μl sitting drops containing 30 mM Mes, pH 6.0, 1 mM $MnCl_2$, 5 mM NaF, 1 mM $NaPP_i$, and 16% 2-methyl-2,4-pentanediol (MPD) and equilibrated against 18 or 20% MPD. The final crystals were grown by macro seeding into 44-μl drops. The crystals were mounted with the above solution plus 29% MPD and frozen in liquid nitrogen. Data to 1.9 Å resolution were collected from a single crystal at $\lambda = 1.0039$ Å, T = 100 K at DESY and integrated as above.

Refinement. The initial phasing of the PPase:Pi_2 structure was from *1wgj*. B factors were set to 15 and the noncrystallographic

Abbreviations: PPases, pyrophosphatases; LBHB, low-barrier hydrogen bond; B-factor, temperature factor; NCS, noncrystallographic symmetry.

Data deposition: The atomic coordinates and structure factors have been deposited in the Protein Data Bank, www.rcsb.org [1e9g and r1e9gsf (PPase:Pi_2) and 1e6a and r1e6asf (PPase:FPPi)].

†Present address: Institute of Chemistry, University of Tromsø, N-9037 Tromsø, Norway.

††To whom correspondence and reprint requests should be addressed at § address. E-mail: Adrian.Goldman@helsinki.fi.

The publication costs of this article were defrayed in part by page charge payment. This article must therefore be hereby marked "*advertisement*" in accordance with 18 U.S.C. §1734 solely to indicate this fact.

BIOCHEMISTRY

Table 1. X-ray statistics

Data collection	PPase:Pi_2	PPase:FPP_i
R_{merge} (I) (last shell)	7.5% (36.3%)	8.1% (24.7%)
Resolution	8.0–1.15 Å	8.0–1.9 Å
Independent observations (multiplicity)	212 495 (3.6)	53 366 (4.5)
Completeness (last shell)	85.4% (75.5%)	97.6% (92.6%)
$I/\sigma I$ (last shell)	11.95 (3.0)	12.58 (4.9)
Refinement		
Reflections $\|F\| > 2\ \sigma$ (F)		87 817
Reflections I ($I > 4\sigma$ I)	205 805 (154 122)	
R_{work}/R_{free} ($F > 4\sigma$ F)	13.6% (11.0%)	15.5/18.2%
Non H atoms	5769	5261
Multiple conformations	202 (3.5%)	106 (2.0%)
Waters	1021	648
Protein B-factors	13.8 Å^2	9.4 Å^2
Phosphate B-factors	8.8 Å^2	9.0 Å^2
Mn^{2+} B-factors	8.7 Å^2	7.8 Å^2
rmsd from target values		
Bond lengths	0.011 Å	0.007 Å
Bond angles	0.026 Å	1.5°
Rigid-bond ADPs	0.05 Å^2	
Approximate isotropic ADPs	0.108 Å^2	

$R_{merge} = \Sigma \mid I_h - \langle I \rangle \mid / \Sigma\ I_h$, where I_h is the measured and $\langle I \rangle$ the average intensity of reflection hkl. R_{free} (7) and R_{work} are conventional crystallographic R-factors ($R = \Sigma \parallel F_{obs} \mid - \mid F_{calc} \parallel / \Sigma \mid F_{obs} \mid$), where F_{obs} is the observed and F_{calc} the calculated structure factor of reflection hkl. B-factors were analyzed with MOLEMAN (G. Kleywegt, unpublished program) and values for rms deviations are from SHELXPRO for PPase:Pi_2 and CNS for PPase:FPPi. ADP, anisotropic displacement parameter.

symmetry (NCS) restrained with a weight of 500. The packing of the two subunits was adjusted by rigid body refinement (7). At 3.0 Å resolution, 6 Mn atoms were added, the structure refined (7) and manually rebuilt (8). Peaks $>4\sigma$ were analyzed and waters, phosphates, and the missing Mn^{2+} added. At 2.3 Å (R_w = 23.4%), grouped B refinement was started and at 2.25-Å NCS weights lowered to 300. Individual temperature factor (B-factor) refinement followed by one round of simulated annealing from 1,000 K gave R_f/R_w of 23.4/20.2% for 8.0–1.7-Å data.

Refinement then continued with the conjugate gradient least squares option in SHELX-97 (9) with default effective standard deviations of 0.015, 0.1, 0.01, and 0.025 to restrain protein chemistry. The refinement was done against all I by using the SWAT bulk solvent correction, but the R_f set of reflections was as above, with R_f/R_w on F of 28.9/21.3%. Refinement to 1.5 Å resolution and addition of restrained anisotropic B-factors lowered R_w to 17.6%. Thirty new waters were added per cycle and those with $U_{ij} > 0.8$ were rejected. At 1.15 Å resolution and R_f/R_w = 18.3/15.3%, anisotropic restraints were released for Mn^{2+}, the structure was refined against all data including the R_f set of reflections, and floating hydrogens were added to all protein residues except H30 Nδ1 in subunits A and B and H87 Nδ1 in A because they cannot be protonated (data not shown). In the last rounds, the BUMP restraint was removed to allow D117 to adjust optimally to the electron density map. The refinement converged to r = 11.01% (Table 1).

The PPase:FPPi structure was refined much as above with NCS restraints (7, 10), starting from the 1.5-Å PPase:Pi_2 structure, with B-factors set to 15, and including Mn^{2+} and the 100 waters with the lowest B-factors. Pyrophosphate was added at 3.5 Å; the two subunits were refined and, at 2.4 Å, water molecules were added. The resolution was increased to 1.90 Å. At this point, the water between M1 and M2 was changed to F^-, waters added, individual B-factor refinement started, and NCS restraints released. An alternate P1 Pi could be added to the B active site and refined so that the occupancy (Pi plus PPi) at the P1 site was 100%. Finally, a B:P2 Pi was added at the same occupancy as B:P1 Pi and Na^+ was added to A-PPase:FPPi. The final R_f/R_w are 18.2/15.5% (Table 1).

Results

Refinement and Selection of Structures for Comparison. The product complex (3) of yeast PPase (PPase:Pi_2) has been refined at 1.15 Å resolution (R = 11.0%), and the fluoride-inhibited substrate complex (PPase:FPPi) at 1.9 Å resolution (R_f/R_w = 18.2/15.5%) (Table 1). The names reflect the differences in active site contents: each additionally contains four Mn^{2+} (M1–M4). M1 and M2 bind before substrate, and M3 and M4 as part of substrate (3). As before (3), the two product phosphates are P1 (leaving group) and P2 (electrophile) and the same names are used for the two phosphorous atoms on pyrophosphate.

Both structures (PPase:Pi_2 and PPase:FPPi) have two independent subunits per asymmetric unit (A and B—e.g., A-PPase:Pi_2 and B-PPase:Pi_2) and both are very similar to the PPase:Pi_2 complex collected at −15°C (1wgj; ref. 3). As previously noted (5), the two independent subunits A and B from a single crystal structure superimpose less well on each other than do A subunits between different structures (e.g., 0.16 Å between A-PPase:Pi_2 and A-PPase:FPPi vs. 0.36 Å between A- and B-PPase:Pi_2). This is due to crystal contacts to the subunit B active site, which confound comparisons between A and B subunits. We therefore focus mainly on the A-subunit active sites.

The key differences among the A-subunit structures pertain to the precise chemical mechanism of the enzyme and are principally the presence of multiple conformations in the active site. In A-PPase:Pi_2, the P1 and P2 phosphates, M3 and E58, N116, and D117 have two conformations, A-PPase:Pi_2^{up} and A-PPase:Pi_2^{down}, named for the orientation of P2 in the active site (Fig. 1). The A-PPase:Pi_2^{down} conformation corresponds to our postulated "immediate hydrolysis product" (3), but was not visible in *1wgj* because the largest change, 1.74 Å, is not resolvable at 2.0 Å. We have thus directly visualized the stable intermediates around the transition state. Unusual interactions around D117 suggest a key role for this residue in catalysis.

The Structure of the A-PPase:FPPi Complex Active Site. In this structure, the pyrophosphate seems to be partially degraded. In B-PPase:FPPi, the occupancy of the P1 and P2 sites is best modeled as 80% PPi and 20% Pi, but A-PPase:FPPi is best modeled as 100% PPi. The active site shows evidence for PPi and an "associated electron density peak" between M1 and M2 (see Figs. 5 and 6, which are published as supplemental data on the PNAS web site, www.pnas.org). We identify the peak as the tight-binding fluoride ion that inactivates the enzyme (11) for three reasons. First, the major conformation of D117 Oδ2 is 0.67 Å further away from this peak than in A-PPase:Pi_2 (Fig. 1) because of the unexpected presence of an Na^+ between the F^- and Oδ2. The Na^+ explains the (F_o–F_c) electron density peak within 2.6 Å of F^- and four other oxygen ligands (Fig. 2*a*). This would be expected if F^- replaced H_2O, with concomitant loss of hydrogen bond donors and increase in negative charge. Second, fluoride inhibition data (12) suggest that F^- binds at this position, and, third, in the D117E variant (5) a carboxylate oxygen of E117 also binds here.

In both subunits, the D117 side chain has two conformations, but the D117^{down} conformation is less pronounced than in the A:PPase:Pi_2 active site (see below): the difference between Oδ1^{up} and Oδ1^{down} is only 1.23 Å. (In B-PPase:FPPi, both D117 and N116 have two conformations, albeit at low occupancy.) Our ultra-high resolution PPase:Pi_2 structure allowed us to identify the alternate conformations in PPase:FPPi that would otherwise have been uninterpretable.

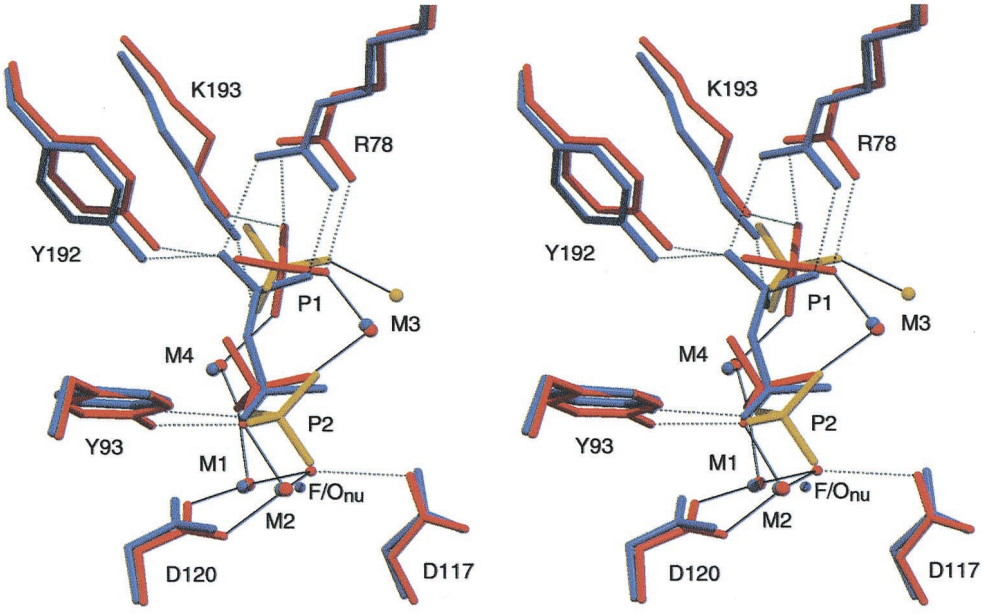

Fig. 1. Three superimposed A-active-site structures. The PPase:FPPi structure is in gray, the PPase:Pi_2^{down} structure is in yellow and the PPase:Pi_2^{up} structure is in orange, showing three separate conformations for the PPi/Pi atoms. All H_2O except the nucleophile O_{nu} are omitted for clarity. The figure shows the similarities between substrate and product binding; the $P2^{up}$ conformation mimics substrate binding, but hydrolyzed P1 moves away. The inline direction from F or O_{nu} toward P2 is always preserved.

Very few other changes are seen in the active site compared with the our original product complex structure (3). The backbone atoms of the residues coordinating the P1 (leaving group) side of the substrate hardly move at all, but there are small side chain adjustments. $Mn_2P_2O_7$, one of the forms of substrate, has 18 lone pairs, of which six are coordinated to metal and nine form hydrogen bonds, six to protein and three to waters (Fig. 2*a*). The tightest interactions are to Y93 Oη (2.51 Å), Y192 Oη, and R78 Nη1 (Fig. 2*a*). The short hydrogen bond to Y93 may provide some of the "steric crowding" that is adduced as part of the mechanism of rate enhancement by LBHBs (13).

The Up and Down Conformations in the A-PPase:Pi_2 Active Site. The current A-PPase:Pi_2^{up} conformation is essentially the same as our earlier structure *1wgj*. However, residues E58, N116, D117, M3, and both phosphates in the 1.15-Å A-PPase active site have similar (minor) occupancies, ranging from 30–35% on the ligand atoms and 43–45% on side chains (Fig. 2 *b–d*). These form the A-PPase:Pi_2^{down} complex linked by similar occupancies and by the conformation of the P2 phosphate, which points "down" toward the base of the active site (Fig. 1). To form A-PPase:Pi_2^{up} from A-PPase:Pi_2^{down}, the P2 phosphate rotates "up" so that one of its oxygens is in approximately the same position as the bridging O in the A-PPase:FPPi complex (Fig. 1). This could occur by preserving the coordination of P2(O2) to M4 and M1, as they are mobile enough to allow the rotation (3), and by losing coordination to M2. $M3^{up}$ is coordinated to P1, P2, and E58, whereas $M3^{down}$ is toward the exit of the active site and is coordinated only to P1 (Fig. 1); we now assign M3 as the "regulatory metal ion" (14).

Importantly, the conformations in A-PPase:Pi_2^{down} and A-PPase:Pi_2^{up} are mutually incompatible; a mixture is sterically impossible. Steric clashes include two clear conformations for the N116 C═O, separated by 1.66 Å at the O, and two overlapped conformations for the D117 CO_2^- (Fig. 3; Fig. 5*b* in supplemental data). The $P2^{down}$ conformation is obviously sterically incompatible with the presence of O_{nu} (Fig. 1), and the A-PPase P1 phosphate also has two conformations (and additional, unmodellable disorder); $P1^{down}$ O3 and $P2^{up}$ O1 (Figs. 1 and 2*b*) are 1.97 Å apart, again incompatible.

In the A-PPase:Pi_2^{down} conformation, there are eight interactions with the P2 phosphate (Fig. 2*b*). P2 should be HPO_4^{2-}, with ten lone pairs (five coordinated by M1-M4), one H-bond donor, presumably P2(O1) to Y93, and two H-bond acceptors (from D117 and K56). The D117Oδ2^{down}–P2(O4) distance is 2.55 Å, short enough to be a potential LBHB (15). In the A-PPase:Pi_2^{up} conformation there are two short interactions, between P2(O1) and P1(O3), and between P2(O4) and Y93 (Fig. 2 *c* and *d*). The latter does not exist in $P2^{down}$, probably because M1 and M2 each coordinate two of the $P2^{down}$ oxygens, pulling $P2^{down}$(O1) away from Y93 (Fig. 2*c*).

Intriguingly, in both A and B subunits the P1(P-O4) and P2(P-O2) bonds appear to have more double bonding character than the other P-O bonds. In both cases, there is more electron density between the atoms than for the other P-O bonds, which appears at this resolution as a tube (Fig. 6 in supplemental data). Such localization of the double bond has been observed in crystalline and fixed environments of hydrated phosphate (16) but, to the best of our knowledge, this is the first time it has been seen in an enzyme active site.

Mechanistic Implications. The A-PPase:Pi_2^{down} conformation corresponds to the "immediate product" intermediate **D** in Scheme 1, as the nucleophilic water is now attached to P2, but still coordinated to M1 and M2. Therefore, it is worth examining the changes between A-PPase:Pi_2^{down} and A-PPase:FPPi, and A-PPase:Pi_2^{down} and A-PPase:Pi_2^{up} for changes that may have mechanistic implications.

The most surprising feature of A-PPase:Pi_2^{down} concerns the interactions centered on N116 (Fig. 3). The distance between N116 O^{down} and D117 Oδ1^{down} is 2.00 Å. This strained interaction appears to be coupled to the motion of Oδ2 toward O_{nu}. The changes start from the H-bond between W100 Nε1 and N116 Oδ1. In the up conformation the H-bond is bent, but in the down conformation N116 Oδ1 moves so that the H-bond shortens, straightens, and strengthens (Fig. 3). This creates steric conflict

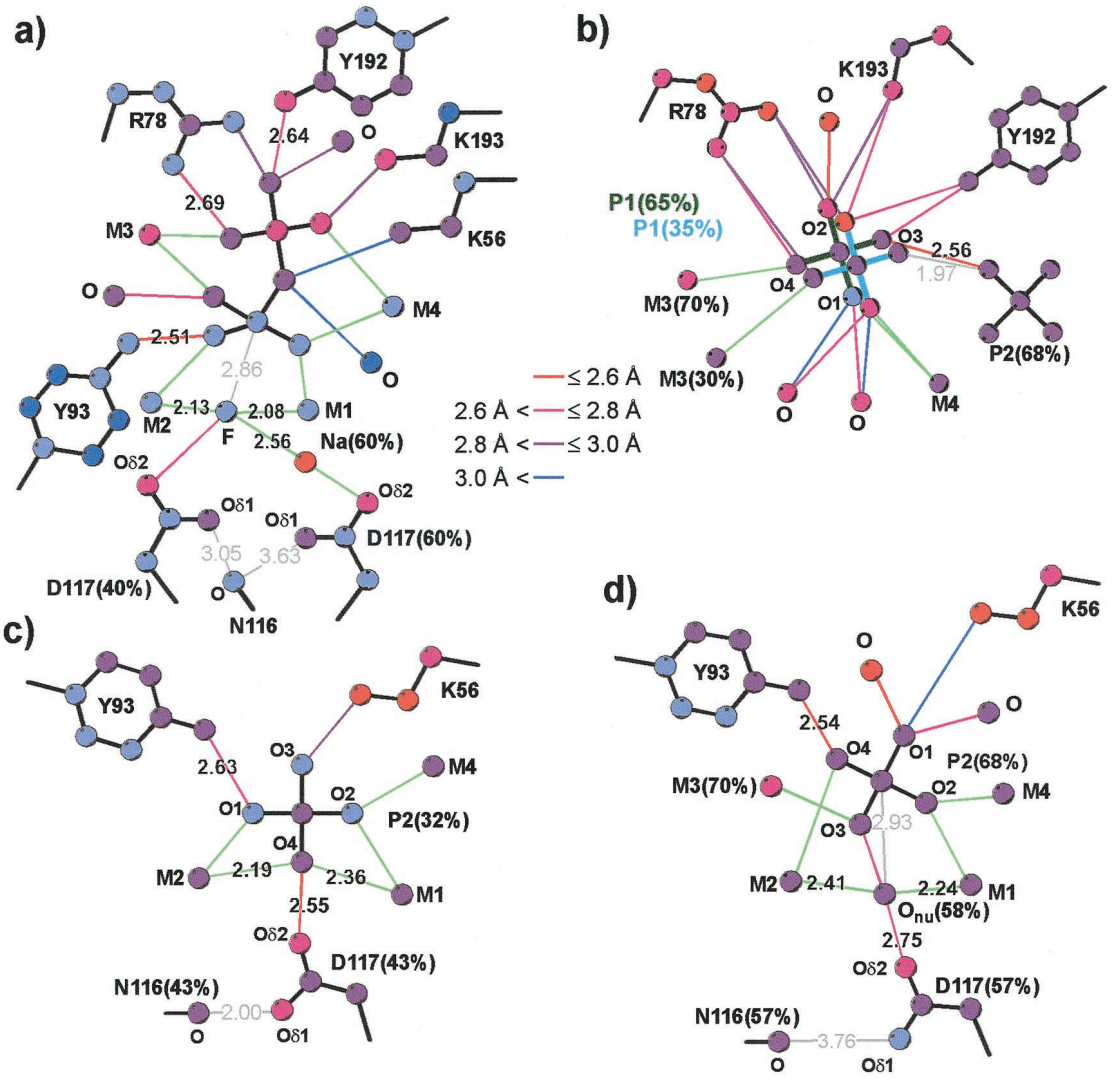

Fig. 2. Geometry in A-PPase active sites. Coordination in: (*a*) F-PPi; (*b*) P1; (*c*) $P2^{down}$; (*d*) $P2^{up}$. Key distances discussed in the text are shown. Atoms are colored by B-factors: dark blue, $< 5Å^2$; light blue, 5–8 $Å^2$; purple, 8–11 $Å^2$; magenta, 11–15 $Å^2$; red, >15 $Å^2$. Hydrogen bonds are color-coded by length, with red for potential LBHBs. P2(O2) in *c* and *d* is believed to remain coordinated to M1 and M4; the labeling of the other oxygens in $P2^{down}$ and $P2^{up}$ is arbitrary. Metal coordination is shown in green and a gray line shows a distance, but without coordination or H-bonding.

with N116 O^{up}, so that N116 C═O rotates up (Fig. 3) to the N116 O^{down} position, and the change propagates along the backbone so that D117 $C\alpha^{up}$ moves to the $C\alpha^{down}$ position. The resultant change in backbone angles favors D117 side chain rotation toward O_{nu} to form an LBHB between D117 Oδ2 and O_{nu} (see *Discussion*). This H-bond is most probably from nucleophilic water (donor) to D117 CO_2^- (acceptor); the issue should be definitively settled by the neutron diffraction structure currently underway.

P1 makes eight interactions in A-PPase:Pi_2^{down}—four are H-bonds to protein, two are H-bonds to water, and two are to M^{2+} (Fig. 2*b*). P1 is pulled away from its position in the A-PPase:FPPi complex by hydrogen bonds to the side chains of R78 and K193: when the A-PPase:FPPi and A-PPase:Pi_2^{down} structures are superimposed, the distance between the P1 phosphorus atoms is 1.3 Å, whereas the distance between the P2 phosphorus atoms is 0.8 Å. The side chains, but *not* the main chains, of R78, K193, K198, and E148 adjust to this motion (Fig. 1).

Discussion

The essentially complete coordination of lone pairs in substrate and product complexes argues for an associative rather than a dissociative mechanism. If the mechanism were dissociative, the charge at P2 would be reduced in the transition state compared with the ground state, resulting in reduced coordination in the A-PPase:FPPi and A-PPase:Pi_2^{down} structures, which bracket the transition state, as compared with the A-PPase:Pi_2^{up} structure. In fact, we see similar P2 coordination in all three structures. Our results are thus consistent with model studies (*vide infra*) showing that metal-coordinated anions attack phosphate monoester dianions via an associative mechanism (17). By contrast, neutral water attack on phosphate monoester dianions proceeds via a dissociative mechanism, both in solution and on enzymes (17–19).

The structures presented here are completely consistent with our earlier proposal that O_{nu} is the nucleophile that directly attacks P2 (3), and not with other suggestions (20); the pyrophosphate conformation allows direct inline attack of O_{nu} on P2 (Fig. 4). The inline direction is preserved even as the nucleophile moves (compare the FPPi and Pi_2^{up} conformations in Figs. 1 and 4). The O-P2-F angle is 175.1° in subunit A and 179.3° in subunit B, and the conformation of P2 in the A-PPase:Pi_2^{down} is as predicted (ref. 3; Figs. 1 and 2).

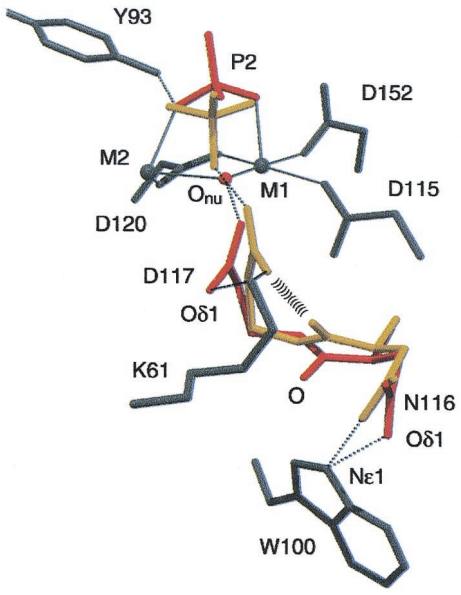

Fig. 3. Nucleophile generation. Residues in A-PPase:Pi_2 are color coded by the conformation in which they occur. Red, up conformation; yellow, down conformation; gray, in both conformations. Metal coordination is shown with solid and H-bonding with dotted lines. As shown, the backbone $^{116}C{=}O$ pushes the D117 CO_2^- toward O_{nu}.

An Extended Mechanism for Pyrophosphatase. A number of lines of evidence suggest, however, that the original pyrophosphatase hydrolysis scheme is not sufficient. First, the two conformations captured in the 1.15-Å structure of A-PPase:Pi_2 correspond to intermediates **D** and **E** in Scheme 1, compared with only one such intermediate in the original scheme. Second, we now have strong evidence for two substrate complexes (**B** and **C** in Scheme 1), based on studies of *S. cerevisiae* inorganic pyrophosphatase (Y-PPase) fluoride inhibition (4), pH-dependence of catalysis (2), and single turnover kinetics (P. Halonen, unpublished data). What inferences, therefore, can be drawn about **B** and **C** based on the structures described here?

In the PPase:Mn_2 complex (pdb *1wgi*; **A** in Scheme 1), M1 and M2 are separated by a two-water molecule bridge (3) but they are separated by a single fluoride ion in the PPase:FPPi (C-analogue) complex. If the structure of PPase:FPPi closely mimics **C**, when does the two-water bridge (**A**) collapse to a one-water bridge (**C**)? We suggest that complex **B** in Scheme 1 contains a two-water bridge between M1 and M2; substrate binds to the two-water bridge structure, which then dehydrates. Similarly, the difference between **D** and **E**, as observed here, is the rehydration of the nucleophile binding site. Our proposal thus creates a pleasing symmetry in the reaction mechanism: **B** is the hydrated version of substrate complex **C**, and **E** is the hydrated version of product complex **D**. It also explains why the pK_a of the ionizable group controlling the **B** to **C** transition is greater than 7, but the pK_a for the **C** to **D** transition is 5.9 (2). The former pK_a would correspond to ionization of one of the water molecules in the two-water molecule bridge leading to loss of the other water molecule. Its pK_a would be much less than 16, but not as low as the pK_a of O_{nu} coordinated to two metal ions, which is 5.9 (2).

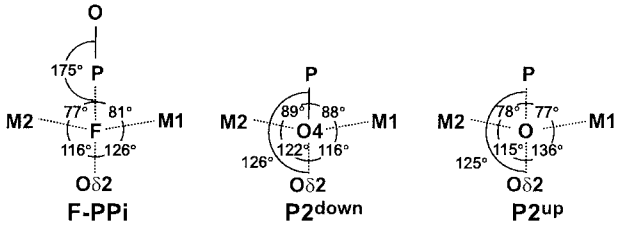

Fig. 4. Angles around F/O_{nu}/P2(O4) in A-PPase FPPi, $P2^{down}$, and $P2^{up}$ complexes. The F-P-O angle is consistent with S_n2 attack, but the angles around the O are not close to tetrahedral.

Sources of Catalytic Power in Pyrophosphatase. What more general lessons about enzyme catalytic power can be drawn? Enzyme catalytic power is in essence due to transition state stabilization: transition state is bound tighter than substrate or product. For an enzyme like PPase that accelerates a reaction 10^{10}-fold, enzyme should bind transition state 10^{10} times tighter than substrate or product. This requires either "passive binding"—molecular recognition through hydrogen bonding, etc.—or "dynamic binding," where special interactions between the catalyst and substrate occur during catalysis (21). There is, however, considerable disagreement about the nature of these "special interactions."

One proposal is orbital steering: reacting groups are placed to maximize the overlap of the highest occupied molecular orbital on the nucleophile and the lowest unoccupied molecular orbital on the electrophile (22). A second proposal is that symmetrical, extremely strong hydrogen bonds form (LBHBs, with X . . . Y distances of 2.4–2.55 Å and ΔH 15–20 kcal/mol; ref. 15). A third, formally related suggestion is that ground-state proton tunneling occurs (23); in such a model, ground-state vibrational forces distort a protein to the point that the "reactant" and "product" curves intersect, allowing rapid tunneling of the proton or hydrogen from reactant to product. A fourth proposal is that substrate binding and transition state binding may not be separable, and so the key element is preorganization of the active site to ensure efficient passage across the transition state (maximization of the transmission factor; refs. 24 and 25). We now examine the structures presented here to see whether they allow any distinction between these proposals.

Orbital Steering. Orbital steering appears unlikely in PPase because, even though the O^{bridge}-P-F angles in PPase:FPPi are very close to 180°, none of the angles around O_{nu} or F are close to tetrahedral, as would be expected for precise orbital alignment (Fig. 4).

Low Barrier Hydrogen Bonds. As mentioned above, O_{nu}, with a pK_a of 5.9 (2), could form an LBHB with D117 Oδ2 because the pK_a of D117 may be as high as 6.25 (2), possibly due to its interaction with the backbone carbonyl of N116. In the A-PPase:Pi_2^{down} active site, the P2-O4 to D117 Oδ2 distance is 2.55 Å and, in the A-PPase:Pi_2^{up} active site, the O_{nu}-D117 Oδ2 distance is 2.75 Å. The distance from D117-$O\delta2^{down}$ to O_{nu} would be only 2.34 Å. Even though this calculation mixes different active site conformations, it shows that D117 Oδ2 approaches the nucleophile very closely.

The strained conformation in the A-PPase:Pi_2^{down} active site, set up by the rigid W100 (see above), further supports this model. The 2.00-Å contact between D117 $O\delta1^{down}$ and N116 O^{down} may sterically compress D117 Oδ2 toward O_{nu} (Fig. 3). A similar mechanism has been proposed for mandelate racemase and other enzymes where dynamic binding during the transition state allows efficient proton transfer (13).

No direct role can be ascribed to the short hydrogen bonds between Y93Oη and P2 oxygens in the A-PPase:FPPi and A-PPase:Pi_2^{up} complexes. The Y93F variant has a k_{cat} 8% of that of wild-type *S. cerevisiae* inorganic pyrophosphatase (Y-PPase; ref. 14) and its role may be to provide additional compression in the active site.

Active Site Preorganization. Canon *et al.* (25) and Warshel (24) suggested that the primary way in which enzymes achieve rate enhancement is by reducing the organizational work for both substrate and environment to reach the transition state: i.e., there is no substantial difference between substrate and transition state binding. We see some evidence to support such a mechanism of rate enhancement for PPase. Neither PPi nor the immediate product A-PPase:Pi_2^{down} fit perfectly. Using the presence of short (and presumably strong) H-bonds as the criterion, the $P2^{up}$ conformation (in PPase:FPPi and PPase:Pi_2^{up}) fits better into the P2-binding site, and the $P1^{up}$ conformation (only in PPase:Pi_2^{up}) fits better into the P1-binding site (Fig. 2). The only conformation between PPase:FPPi and PPase:Pi_2^{down} that might simulate the up-conformation at both P1 and P2 is the transition state, consistent with preorganization of the active site.

In addition, the lack of substantial backbone movement between substrate and product in the ligands binding P1 may help achieve rapid catalysis. Like the shock absorbers on a car, the side chains may isolate the rest of the protein from the active site "protein quake" [cf. myoglobin (26)], thus allowing the active site to respond faster. Consistent with this, motion in the active site is split in two. Between A-PPase:FPPi and A-PPase:Pi_2^{down}, only side chains move in the P1 site but the P1 phosphorus moves by 1.3 Å; but main chain and side chain movement occurs in the P2 site, where the P2 phosphorus moves only 0.8 Å. Conversely, between A-PPase:Pi_2^{down} and A-PPase:Pi_2^{up} there is only slight motion at P1, but main chain motion at P2.

Some of the vibrational motions in the active site, as evidenced by the anisotropic B-factors, also appear to be arranged to achieve efficient catalysis. This ground-state effect may enhance the rate of reaction. For instance, in A-PPase:Pi_2^{up} the major anisotropic motion of O_{nu} is in the M1 and D117 Oδ2 directions. In addition, D117 O$\delta2^{up}$ shows anisotropic motion toward D117 O$\delta2^{down}$.

Ground-State Proton Tunneling. Ground-state-based proton tunneling from O_{nu} to D117 may also play a role, as has been proposed for hydrogen tunneling in methylamine dehydrogenase (23). The motion described above compresses D117 O$\delta2^{up}$ toward the catalytically active D117 79 $\delta2^{down}$ conformation, thus allowing efficient tunneling between O_{nu} and D117 and generation of the nucleophile. This argument is in some ways formally analogous to the suggestion that an LBHB forms between D117 Oδ2 and O_{nu}; in both models, rate enhancement is due to compression of the heavy atoms in the hydrogen bond.

These structures provide a framework to test current hypotheses of enzymological rate enhancement in PPases, lending support to LBHBs and ground-state effects in catalysis but not to orbital steering. They also demonstrate that significant mechanistic observations can be made from ultra-high resolution structures of enzyme substrate/product complexes. For a nonallosteric enzyme like PPase, the structures are as relevant as those obtained by time-resolved crystallography because a mixture of mechanistically relevant conformations can be found on the enzyme. We are thus moving closer to our goal of understanding phosphoryl transfer in PPases at the quantum mechanical level.

We thank R. Andersen, M. Merckel, T. Kajander, and P. Vahakoski. This work was supported by the Academy of Finland (Grant 4310 to A.G. and R.L.; 42979 to P.H.; and a training grant to V.T.), and the European Union TMR/LSF to European Molecular Biology Laboratory Hamburg Outstation (ERBFMGECT980134).

1. Baykov, A. A., Cooperman, B. S., Goldman, A. & Lahti, R. (1999) in *Progress in Molecular and Subcellular Biology*, eds. Schröder, H. C. & Müller, W. E. G. (Springer, Heidelberg), Vol. 23, pp. 127–150.
2. Belogurov, G. A., Fabrichniy, I. P., Pohjanjoki, P., Kasho, V. N., Lehtihuhta, E., Turkina, M. V., Cooperman, B. S., Goldman, A., Baykov, A. A. & Lahti, R. (2000) *Biochemistry* **39,** 13931–13938.
3. Heikinheimo, P., Lehtonen, J., Baykov, A., Lahti, R., Cooperman, B. S. & Goldman, A. (1996) *Structure* **4,** 1491–1508.
4. Baykov, A. A., Fabrichniy, I. P., Pohjanjoki, P., Zyryanov, A. B. & Lahti, R. (2000) *Biochemistry* **39,** 11939–11947.
5. Tuominen, V., Heikinheimo, P., Kajander, T., Torkkel, T., Hyytiä, T., Kapyla, J., Lahti, R., Cooperman, B. S. & Goldman, A. (1998) *J. Mol. Biol.* **284,** 1565–1580.
6. Otwinowski, Z. & Minor, W. (1997) *Methods Enzymol.* **276,** 307–326.
7. Brünger, A. T. (1987) X-PLOR, A System for X-Ray Crystallography and NMR (Yale Univ. Press, New Haven, CT), Version 3.1.
8. Jones, T. A., Zou, J.-Y., Cowan, S. W. & Kjeldgaard, M. (1991) *Acta Crystallogr. A* **47,** 110–119.
9. Sheldrick, G. M. & Schneider, T. R. (1997) *Methods Enzymol.* **277,** 319–343.
10. Brünger, A. T., Adams, P. D., Clore, G. M., DeLano, W. L., Gros, P., Grosse-Kunstleve, R. W., Jiang, J.-S., Kuszewski, J., Nilges, M., Pannu, N. S., *et al.* (1998) *Acta Crystallogr. D* **54,** 905–921.
11. Baykov, A. A., Bakuleva, N. P., Nazarova, T. I. & Avaeva, S. M. (1977) *Biochim. Biophys. Acta* **481,** 184–194.
12. Pohjanjoki, P., Fabrichniy, I. P., Kasho, V. N., Cooperman, B. S., Goldman, A., Baykov, A. A. & Lahti, R. (2000) *J. Biol. Chem.*, in press.
13. Frey, P. A. & Cleland, W. W. (1998) *Bioorg. Chem.* **26,** 175–192.
14. Pohjanjoki, P., Lahti, R., Goldman, A. & Cooperman, B. (1998) *Biochemistry* **37,** 1754–1761.
15. Cleland, W. W., Frey, P. A. & Gerlt, J. A. (1998) *J. Biol. Chem.* **273,** 25529–25532.
16. Mighell, A. D., Smith, J. P. & Brown, W. E. (1969) *Acta Crystallogr. B* **25,** 776–780.
17. Cleland, W. W. & Hengge, A. C. (1995) *FASEB J.* **9,** 1585–1594.
18. Admiraal, S. J. & Herschlag, D. (1995) *Chem. Biol.* **2,** 729–739.
19. Admiraal, S. J., Schneider, B., Meyer, P., Janin, J., Veron, M., Deville-Bonne, D. & Herschlag, D. (1999) *Biochemistry* **38,** 4701–4711.
20. Harutyunyan, E. H., Kuranova, I. P., Vainshtein, B. K., Höhne, W. E., Lamzin, V. S., Dauter, Z., Teplyakov, A. V. & Wilson, K. S. (1996) *Eur. J. Biochem.* **239,** 220–228.
21. Kirby, A. J. (1996) *Angew. Chem. Int. Ed. Engl.* **35,** 707–724.
22. Mesecar, A. D., Stoddard, B. L. & Koshland, D. E., Jr. (1997) *Science* **277,** 202–206.
23. Sutcliffe, M. J. & Scrutton, N. S. (2000) *Philos. Trans. R. Soc. London A* **358,** 367–386.
24. Warshel, A. (1998) *J. Biol. Chem.* **273,** 27035–27038.
25. Cannon, W. R., Singleton, S. F. & Benkovic, S. J. (1996) *Nat. Struct. Biol.* **3,** 821–833.
26. Ansari, A., Berendzen, J., Bowne, S. F., Frauenfelder, H., Iben, I. E., Sauke, T. B., Shyamsunder, E. & Young, R. D. (1985) *Proc. Natl. Acad. Sci. USA* **82,** 5000–5004.